VISUALIZING CHANGES IN VESSEL WALL DYNAMICS DUE TO STENT-GRAFTING IN THE AORTIC ARCH

Ernst Schwartz[⋆] *Johannes Holfeld*[†] *Martin Czerny*[◇] *Georg Langs*[⋆]

[⋆] Computational Imaging and Radiology Lab, Department of Radiodiagnostics, Medical University of Vienna
[†]Deptartment of Cardiac Surgery, Innsbruck Medical University
[◇]Department of Cardiovascular Surgery, Bern University Hospital

ABSTRACT

The thoracic aorta is an anatomical structure that is subject to constant motion. Stent-grafting changes the deformation patterns on the vessel surface, and the nature of these changes is suspected to correlate with treatment outcome. However, they are currently only poorly understood. We propose a method for quantifying the changes in vessel motion caused by stent-grafting in the aortic arch. For this, we automatically build a surface model of the vessel and its movement from gated computed tomography sequences that depict the deformation of the thoracic aorta during the cardiac cycle. We reconstruct trajectories corresponding to the displacement of a dense sampling of the vessel surface. From these, we construct a manifold of vessel motion patterns. Models acquired before and after stent-grafting are registered and we analyze the changes to the deformation in the embedding space. Results for four clinical cases indicate that the local density in the embedding space is a marker of local deformation complexity, and sites of potential complications.[1]

Index Terms— vascular imaging, treatment outcome, manifold methods

1. INTRODUCTION

Understanding the changes that are caused by vascular interventions such a stent-grafting is crucial for risk assessment in the individual patient, and for understanding the effects of device designs. Among other approaches the task of quantitatively determining the effects of vascular interventions is commonly performed via patient-specific Computational Fluid Dynamics (CFD) studies [1]. Commonly, the only dynamic taken into account by these models is the interaction of blood flow with the simulated vessel. While this simplification holds for most vessels in the human body, it is not a viable assumption for the thoracic aorta that is subject to strong movement due to its closeness to the heart. Interventions in that region are amongst the most complicated and potentially hazardous and therefore call for detailed observation.

We propose a method to analyze the effects of stent-grafting on global and local deformation patterns of the aorta. To obtain a metric that reflects the often subtle changes to the motion trajectories, we learn a manifold of vessel motion. In this manifold we detect localized changes, and measure how properties such as motion coherence are affected by the implant.

1.1. Related Work

Motion analysis is an active area of research in computer vision. It has been applied most notably to human pose and motion recognition in the context of surveillance and entertainment applications [2]. The approaches used for this class of problems range from task-specific explicit models to purely data-driven methods. A common way for describing the complex space of natural motion is by assuming that the observed data lies on a low-dimensional manifold embedded in a high-dimensional space [3]. For a recent exhaustive overview of the field, see [4].

Motivated by the application to coronary arteries, the study of vessel movement however has largely been limited to analyzing the deformations of vessel centerlines in Euclidean space [5]. In these applications, scalar values describing vessel movement and the induced strain are derived from temporal radiographic imaging techniques. In more recent work the vessel surface is considered [6, 7] which forms a precursor to the present paper.

In this paper, we propose to apply dimensionality reduction methods to the problem of vessel movement. We first describe the proposed manifold method in detail in section 2. We then apply it in section 3 to 4 clinical cases to show the effects of stent-grafting in the aortic arch. A discussion of the results concludes the paper in section 4.

2. A MANIFOLD OF VESSEL MOTION

For each patient, we extract the motion of the aorta surface from pairs of Computed Tomography Angiography (CTA) se-

[1]This work was partly funded by the OeNB (13497, AORTAMOTION), the European Union (257528, KHRESMOI), and the Austrian Sciences Fund (P 22578-B19, PULMARCH).

quences acquired before (S) and after the intervention (T). The trajectories of a dense sampling of the vessel surface are used to build a manifold of vessel motion or *motion vocabulary*. It allows for a comparison of motion patterns and a quantitative assessment of changes caused by the stent-graft. We show how this embedding reflects the effects of stent-grafting and could be used for follow-up assessment of that and other interventions.

2.1. Extracting Vessel Motion

For each patient we obtain a pair of ECG-gated CTA sequences. In the following, S denotes the sequence acquired before and T that after implantation of a stent-graft in the aortic arch. Each sequence consists of n retrospectively reconstructed volumes or frames $\{F^1 \dots F^n\}$. In all discussed cases, $n = 10$. Across acquisitions, each frame corresponds to the same phase in the cardiac cycle. The patients are injected with 110ml Iomeron 400 to enhance the contrast in the vessel lumen.

2.1.1. Registration

For each sequence, pair-wise Free-Form Deformation (FFD) [8] with Sum of Squares Differences (SSD) as similarity measure is used to register the first frame to all remaining frames in a sequence. This defines a series of deformation fields $\{\mathcal{S}^i = F^1 \rightarrow F^i, i = 2 \dots n\}$ and $\{\mathcal{T}^i\}$ corresponding to all frames in the sequences S and T respectively.

2.1.2. Segmentation

The contrast agent in the patient's blood allows the segmentation of the lumen of the aorta in the first frames of S and T using a level-set method [9]. From the resulting 0-level set of each segmentation, we compute sets of surface vertices $\mathbf{V}_S = \{\mathbf{v}_1, \dots, \mathbf{v}_k\}$ and $\mathbf{W}_T = \{\mathbf{w}_1, \dots, \mathbf{w}_l\}$ respectively.

2.1.3. Matching Pre- and Post-Intervention Surfaces

To be able to compare vessel movement before and after stent-grafting, corresponding surface sampling points in S and T are required. We obtain them by computing a mapping $\Theta(\mathbf{V}_S, \mathbf{W}_T) = \mathbf{V}_T$ between the surface point sets in the first frame of the two vessel models using non-rigid Coherent Point Drift (CPD) registration [10]. Θ is computed by optimizing the parameters of a Gaussian Mixture Model (GMM) with initial centers $\mathbf{V}_S$ to fit $\mathbf{W}_T$. This results in a new set of sampling locations $\mathbf{V}_T$, where each point $\mathbf{v}_{i,T}$ in T corresponds to a position $\mathbf{v}_{i,S}$ in S. Consequently, the number of model points $\sharp\{\mathbf{v}_S\} = \sharp\{\mathbf{v}_T\} = k$ is equal. For the cases presented in this paper, $k \approx 1000$.

2.1.4. Vessel Motion Trajectories

Having computed corresponding static surface models $\mathbf{V}_S$ and $\mathbf{V}_T$ and the series of deformation fields $\{\mathcal{S}^i\}$ and $\{\mathcal{T}^i\}$ allows for the extraction of trajectories of local regions of the aorta in S and T respectively. For this, we aggregate the displacement at the model points $\mathbf{V}_S$ over time through $\{\mathcal{S}^i\}$ as $\mathbf{V}_S^i = \mathbf{V}_S^{i-1} + \mathcal{S}^{i-1}(\mathbf{V}^{i-1}), i = 2 \dots n, \mathbf{V}_S^1 = \mathbf{V}_S$. The same procedure is applied to $\{\mathcal{T}^i\}$ with $\mathbf{V}_T^1 = \mathbf{V}_T$. This results in sets of pairwise corresponding trajectories $\mathbf{P} = \{\mathbf{V}_S^1 \dots \mathbf{V}_S^n\}$ and $\mathbf{Q} = \{\mathbf{V}_T^1 \dots \mathbf{V}_T^n\}$. We fit a smoothing spline to each trajectory $\mathbf{p}_j \in \mathbf{P}$ and $\mathbf{q}_j \in \mathbf{Q}$ and resample it at the same resolution n. The matched trajectories are thus related by

$$\begin{matrix}(\mathbf{p}_j, \mathbf{q}_j) \\ \mathbf{p}_j, \mathbf{q}_j \in \mathbb{R}^{3n}\end{matrix} \tag{1}$$

where $j = 1 \dots k$ is an index over all sampling points.

2.2. The Intrinsic Space of Vessel Motions

Instead of directly using their Euclidean distance, or other a priori chosen features, between trajectories, we learn a space that represents the variability of the observed deformation. We compute a joint embedding Ψ of the trajectories $\mathbf{p}_j$ and $\mathbf{q}_j$ representing the movement of the thoracic aorta in a d-dimensional space ($d < 3n$). The rationale is that while the Euclidan distance between trajectories is sensible if they are similar, it is far less informative for trajectories that differ strongly.

By testing for the portion of the data explained by an embedding in a given dimension a value for d can be estimated. In order to limit the influence of noise to the process we chose $d = 6$ which we found to be the lowest dimensionality able to account for 99.95% of the variability in the data in all 4 cases.

2.2.1. Building the Manifold of Vessel Motion

We employ a local embedding method (Locally Linear Embedding - LLE [11]) to compute the embedding. In order to remove the information of location in space, each trajectory is centered around its center of gravity. The resulting manifold $\mathcal{M}$ consists of points α_j and β_j and can be described as

$$\begin{aligned} \mathcal{M} \quad &= \quad \Psi\left(\{\mathbf{p}_j | j = 1 \dots k\} \cup \{\mathbf{q}_j | j = 1 \dots k\}\right) \\ \Psi: \quad & \mathbb{R}^{3n} \longmapsto \mathbb{R}^d \\ & \mathbf{p}_j \mapsto \boldsymbol{\alpha}_j = \Psi(\mathbf{p}_j), \\ & \mathbf{q}_j \mapsto \boldsymbol{\omega}_j = \Psi(\mathbf{q}_j) \end{aligned} \tag{2}$$

2.2.2. Structure of the Manifold

As can be seen in equation (2), the embedding of the trajectories $\mathbf{p}$ and $\mathbf{q}$ is computed jointly without information about their provenance from S ($\mathcal{M}_{\boldsymbol{\alpha}}$) or T ($\mathcal{M}_{\boldsymbol{\omega}}$). Nonetheless, this paired structure is present in the embedding space as

$$\begin{matrix}\mathcal{M} = \mathcal{M}_{\boldsymbol{\alpha}} \cup \mathcal{M}_{\boldsymbol{\omega}} \\ \sharp\{\mathcal{M}_{\boldsymbol{\alpha}}\} = \sharp\{\mathcal{M}_{\boldsymbol{\omega}}\} = k\end{matrix} \tag{3}$$

2.3. Evaluating the Effects of Stent-Grafting

The manifold $\mathcal{M}$ represents the information about the deformation of the aorta in a compact manner. Changes induced in the movement of the vessel can be observed and described in that space. We propose to describe changes in the local motion properties using the local density in the embedding space at the positions of the trajectories.

Similar trajectories lie closer on the manifold than differing ones. Regions with high density in the embedding space therefore correspond to clusters of similar, coherent motion. As the implanted stent-graft tends to move more rigidly than the surrounding tissue, we expect to find the sampling points corresponding to the stented area to lie closer together on the manifold after the intervention than before.

3. RESULTS

We apply the proposed method to 4 clinical cases in which a stent-graft has been implanted in the aortic arch following supra-aortic rerouting [12]. To allow for an easier interpretation of the results, we plot the measurements on the vessel wall in a 2D representation where the vessel surface has been *unfolded* radially following the vessel centerline.

The change in density at the model points in the embedding space, along with its minimum, maximum and median along the vessel centerline is shown in Figure 1. The densities have been computed via kernel density estimation using case-specific kernels. The anisotropic kernel sizes are chosen automatically and vary with the estimated standard deviation in each dimension of the embedding space. We use only $\mathcal{M}_\alpha$ to estimate the density for the pre-intervention points $\boldsymbol{\alpha}$, while $\mathcal{M}_\omega$ is used to estimate the density for $\boldsymbol{\omega}$. In order to allow intra-case comparisons, the differences have been normalized by the respective mean densities of $\mathcal{M}_\alpha$.

3.1. Observed changes in subspace density

The mean change in embedding space density in the stented part of the aorta is 0.05 for case 1 and -0.29 in case 2 (see Figures 1a and 1b). In both cases, the low values at the beginning of the stent near the aortic valve indicate an inhomogenization of the vessel movement in that area. This behavior was expected and can be explained by the influx of blood into the wider opening of the stent as well as the different properties of the vessel wall and the stent-graft.

The changes in vessel movement in cases 3 and 4 (Figures 1c and 1d) exhibit a starkly different characteristic. In both cases a substantially longer stent-graft was implanted, that was positioned closer to the heart. Case 3 shows an overall increase in embedding-space density in the stented region of 2.43 while that of case 4 is 1.45. The homogenization is not limited to the stented area in these cases. In fact, the whole of both vessels are indicated to move more coherently due to the intervention. Also, no decrease in motion coherence at the beginning of the stent-graft can be observed.

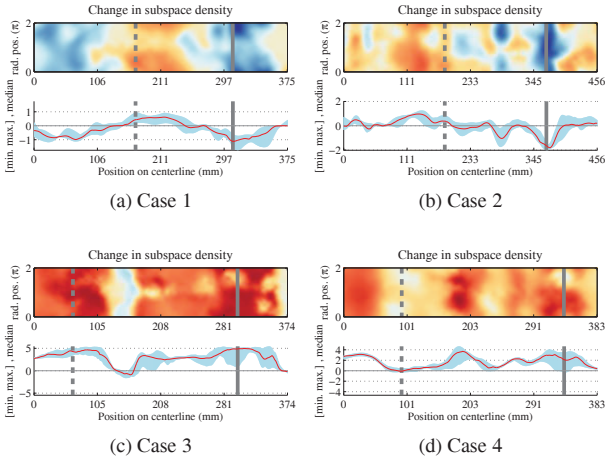


Fig. 1: Changes in densities of the embedding spaces of the 4 presented cases, along with their minima, maxima and medians in circumferential direction along the vessel centerline. The stent-grafts are indicated by continuous (closer to the aortic valve) and dotted lines.

3.2. Influence of stent-graft size

We hypothesize that the observed behavior is due to the relative length and placement of the prosthesis. Because the stented area begins closer to the heart in both cases 3 and 4, the direction of the upper part of the stent is more in line with the general direction of blood flow. These factors seem to influence the effects of the intervention. Figure 2 shows the change in embedding-space density in all 4 cases (left axis), along with the relative portion of the aorta that was subjected to stent-grafting and the relative position of the prosthesis in the vessel starting from the aortic valve (right axis). It illustrates that the density change characteristics correspond to the two classes of prostheses positions and lengths (cases 1 and 2 vs. cases 3 and 4).

The increase in embedding-space density is higher when more than 50% of the thoracic aorta have had to be supported by a stent-graft and it lies closer to the heart. Quantitatively, the correlation between mean change in embedding space density of points corresponding to the stent-graft and the relative location of the beginning of the stent is -0.98. The correlation of the proposed density measure with the relative length of the stent is 0.91.

These observations indicate a relationship between the mobility of the aorta and the length and location of the stented area. The relationship becomes quantifiable by the measurements based on the motion manifold.

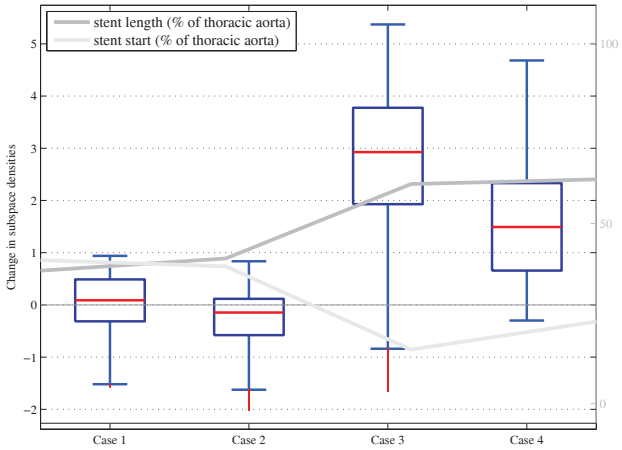


Fig. 2: Comparison of the changes in density of embedding space in the stented area of the aorta in the 4 presented cases (left axis) along with the length and start of the stent relative to the length of the pictured aorta.

4. CONCLUSION

In this paper, we introduce a method to describe the motion of the thoracic aorta and changes caused by treatment. The basis of the measurement is a manifold learned from the data that represents local vessel movement. We use the manifold to quantify effects of stent-grafting in the highly dynamic region of the aortic arch onto vessel movement.

Initial results indicate that the proposed *motion vocabulary* holds valuable information about differences in vessel movement. The density of the embedding space of the manifold can be used to assess the influence of stent-grafting on the motion of the aorta. While the available sample size of 4 cases is relatively small, our results give a clear indication of the influence of the length and position of the prosthesis on the effect of the intervention. The observed fine-grained patterns observable via the manifold metric motivate the use of the proposed method to assess the movement of the aorta in greater detail than a Euclidean metric on the trajectories.

5. REFERENCES

[1] Guanglei Xiong, C. Alberto Figueroa, Nan Xiao, and Charles A Taylor, "Simulation of blood flow in deformable vessels using subject-specific geometry and spatially varying wall properties," *International Journal of Numerical Methods in Biomedical Engineering*, vol. 27, pp. 1000–1016, 2010. 1

[2] W Hu, T Tan, L Wang, and S Maybank, "A survey on visual surveillance of object motion and behaviors," *Systems, Man, and Cybernetics, Part C: Applications and Reviews, IEEE Transactions on*, vol. 34, no. 3, pp. 334–352, 2004. 1

[3] A Goh and R Vidal, "Segmenting motions of different types by unsupervised manifold clustering," *2007 IEEE Conference on Computer Vision and Pattern Recognition*, pp. 1–6, 2007. 1

[4] T.B Moeslund, A Hilton, and V Kruger, "A survey of advances in vision-based human motion capture and analysis," *Computer Vision and Image Understanding*, vol. 104, no. 2-3, pp. 90–126, 2006. 1

[5] D Kang, DC Suh, and JB Ra, "Three-dimensional blood vessel quantification via centerline deformation," *IEEE Transactions on Medical Imaging*, vol. 28, no. 3, pp. 405–414, 2009. 1

[6] Georg Langs, Nikos Paragios, Pascal Desgranges, Alain Rahmouni, and Hicham Kobeiter, "Learning deformation and structure simultaneously: In situ endograft deformation analysis," *Medical Image Analysis*, vol. 15, no. 1, pp. 12–21, Feb 2011. 1

[7] E Schwartz, R Gottardi, J Holfeld, C Loewe, M Czerny, and G Langs, "Evaluating deformation patterns of the thoracic aorta in gated cta sequences," *Biomedical Imaging: From Nano to Macro, 2010 IEEE International Symposium on*, pp. 21–24, 2010. 1

[8] D Rueckert, LI Sonoda, C Hayes, DLG Hill, MO Leach, and DJ Hawkes, "Nonrigid registration using free-form deformations: application tobreast mr images," *Medical Imaging, IEEE Transactions on*, vol. 18, no. 8, pp. 712–721, 1999. 2

[9] JA Sethian, *Level set methods and fast marching methods*, Cambridge University Press, 1999. 2

[10] Andrij Myronenko and Xubo Song, "Point set registration: Coherent point drift," *IEEE Transactions in Pattern Analysis and Machine Intelligence*, vol. 32, no. 12, pp. 2262–2275, 2010. 2

[11] ST Roweis and LK Saul, "Nonlinear dimensionality reduction by locally linear embedding," *Science*, vol. 290, no. 5500, pp. 2323–2326, 2000. 2

[12] Roman Gottardi, Martin Funovics, Nella Eggers, Alexander Hirner, Marion Dorfmeister, Johannes Holfeld, Daniel Zimpfer, Maria Schoder, Konstantin Donas, Ernst Weigang, Johannes Lammer, Michael Grimm, and Martin Czerny, "Supra-aortic transposition for combined vascular and endovascular repair of aortic arch pathology," *Annals of Thoracic Surgery*, vol. 86, no. 5, pp. 1524–1529, 2008. 3